JOURNAL OF MATERIALS SCIENCE: MATERIALS IN MEDICINE 11 (2000) 163–174

The prediction of polyethylene wear rate and debris morphology produced by microscopic asperities on femoral heads

C. M. MCNIE, D. C. BARTON, E. INGHAM*, J. L. TIPPER*, J. FISHER‡
*School of Mechanical Engineering and *Department of Microbiology, The University of Leeds, Leeds, LS2 9JT, UK*

M. H. STONE
Department of Orthopaedic Surgery, Leeds General Infirmary, Leeds, LS1 3EX, UK

Counterface damage in the form of scratches, caused by bone cement, bone or metallic particles, has been cited as a cause of increased wear of ultra-high molecular weight polyethylene (UHMWPE) acetabular cups. It is known that high levels of particulate wear debris lead to osteolysis. Surface damage was characterized in a series of explanted Charnley femoral heads. The heads had a mean scratch height of 1 μm with a mean aspect ratio (defined as height divided by half width) of 0.1. Wear discs were artificially scratched using these scratch geometries as a guide. In addition, the scratch geometries were incorporated into a finite element model of a stainless steel asperity repeatedly sliding over UHMWPE under conditions similar to those in an artificial hip joint. Wear tests showed a strong correlation between the average cross-sectional area of the scratch lip above the mean zero line and the measured wear factor. The finite element model predicted increases in the area of UHMWPE suffering plastic strain with increases in the cross-sectional area of the asperity above the mean line. Analysis of the wear debris showed the mode of the particle size was 0.01–0.5 μm for all cases. The morphology of the particles varied with aspect ratio of the asperity, with an increased percentage mass of submicrometer-sized debris with increased scratch lip aspect ratio. The finite element results predicted that the maximum surface strains would increase with increasing asperity aspect ratio. Examination of the worn UHMWPE pin surfaces showed an association between increased surface damage, probably due to high surface strains, and increased aspect ratio. The large areas of surface plastic strain predicted for asperities with high cross-sectional areas above the mean line offer an explanation for the positive correlation between wear rate and the average cross-sectional area of the scratch lip material. The higher surface strains predicted for the higher aspect ratios may explain the increased percentage mass of biologically active submicrometer-sized wear particles found for scratch lips with higher aspect ratios.

1. Introduction

Total hip arthroplasties are the most successful and common joint replacements. Around 80% of total hip replacement (THR) joints are successful for between 15 and 20 years. The popularity of this type of surgery is based on the immediate relief of pain and the excellent recovery of movement. However, since these joints are now being implanted in increasing numbers into younger people, they must be durable for at least 20 years. The most common material combination of the THR is a hard metal or ceramic femoral head and a plastic, usually ultra-high molecular weight polyethylene (UHMWPE), acetabular cup. Currently it is believed that the wear of the UHMWPE component, and in particular wear debris induced osteolysis, is a cause of premature failure of replacement hips.

There have been many theories as to the origins of loosening and failure of THRs, including the effect of stress shielding, cement fatigue, particles of acrylic bone cement and particulate wear debris, all of which may lead to bone resorption. The present view, which takes into account the fact that bone resorption often occurs late in the artificial joint's life [1], is that particulate wear debris is the major cause of osteolysis in THR joints. This may of course occur in conjunction with stress shielding and cement fatigue, which may create pathways for wear debris particles to reach the bone–biomaterial interface. The proposed mechanism leading to bone resorption is

‡Author to whom correspondence should be addressed.

that phagocytic cells (macrophages) engulf the foreign wear particles present in the periprosthetic tissue. The macrophages are activated by the particles and release chemical mediators (cytokines), which induce osteolysis.

In vitro tests [2] of wear debris from retrieved tissue surrounding UHMWPE cups have shown that the particles are a potent stimulus of cytokine production by macrophages. It has been shown that particles less than 5 μm in mean dimension stimulated macrophages and these were the most important in the production of osteolytic cytokines [3]. Moreover, retrieved tissues have been found to contain significant volumes of UHMWPE less than 1 μm in size [4, 5]. This microscopic wear debris has been associated with femoral counterfaces with a roughness, R_a, in the range 0.01–0.1 μm [6].

The precise wear mechanisms that occur in THRs are not fully understood and this study aims to add to the present knowledge. It is believed that macroscopic abrasive wear is dependent on the radius of the defect on the counterface, with the mechanism changing from ploughing to wedge forming to cutting mode as the radius decreases [7]. During abrasive wear, the wear particles are either wedge-shaped or ribbon-like. This wear process may occur in UHMWPE prostheses, which would explain the presence of the larger particles, over 100 μm, found *in vivo* [8]. For microscopic wear, it has been postulated that during relative sliding, microscopic asperities on the femoral counterface repeatedly deform the polymer surface, elastically and plastically [9]. It is possible that the level of plastic (i.e. non-recoverable) strain induced may be much higher than for a smooth contact, leading to a rapid build-up of damage and microcracking in the polymer. The wear particle is finally produced by fatigue crack growth and, as the amplitude of the stress field increases, fewer cycles are required to cause this. Before escaping from the contact, the particle can act as a third body, damaging and wearing both surfaces. Due to the high stresses present in this type of contact, the particle may also be deformed, either by altering its morphology, breaking up into smaller particles or alternatively aggregating into larger particles. Therefore it is postulated that the femoral head surface topography and in particular the presence of defects on this surface will influence the number and morphology of micrometer- and submicrometer-size particles generated [8].

Over the years, there have been a number of finite element stress analyses of the UHMWPE component in artificial joints. More recently, there have been advanced simulations of cyclic loading by a rigid indentor sliding over UHMWPE [10]. These studies have been primarily concerned with the stress fields in the bulk polymer and have not generally modeled the surface asperities. The present authors [11] have recently developed a finite element model to investigate plastic strain fields at the surface of UHMWPE for real asperity geometries. However, the models have not previously been developed for repeated cyclic sliding as occurs in the hip or for the presence of multiple scratch lips. Most importantly, experiments have not been undertaken to support such theoretical models. In THR joints, in which the generation of micrometer size UHMWPE wear particles appears to be a critical determinant of osteolysis, an understanding of the microscopic wear mechanisms and the development of qualitative (if not quantitative) relationships between realistic surface topographies, material properties and wear rates are of fundamental importance.

The aim of the present study was therefore to investigate the effect of the geometry of femoral head surface defects on the wear, wear debris and near-surface strain fields in the UHMWPE through both experimental and finite element analysis (FEA) methods. This was achieved by carrying out laboratory wear tests using different scratch lip geometries and analysis of the resulting wear surfaces and wear debris. This experimental analysis was supported by using a non-linear finite element model of typical asperity contacts, which predicted the surface and subsurface plastic strains in the UHMWPE. The combination of the experimental results and theoretical predictions has allowed the development of relationships between asperity geometries, plastic strains, wear rates and wear particle morphologies.

2. Materials and methods

Experiments were carried out to study the effect of asperity geometry on wear rate and debris morphology.

A twin-headed tri-pin-on-disc tribometer was used, which enabled two discs to be run at the same time with the twin head driven by the same motor from a central position. The rotating motion of each disc was unidirectional. Each head contained three pins equispaced on a 75 mm pitch circle diameter in the stationary pin holder with a fourth pin not in contact with the rotating disc used as a control for water absorption during the test. The discs and pins were enclosed in a bath to enable the test to be run wet. Each head was enclosed by a perspex housing to prevent contamination. The loading of the head was by dead-weights applied via a cantilever arm.

Cylindrical pins (9.5 mm diameter) with a conical end and a 3 mm wear face were manufactured from GUR 1120 UHMWPE compression molded sheet. The discs were manufactured from surgical grade stainless steel with a nominal diameter of 75 mm and an initial surface roughness, $R_a < 0.02$μm.

2.1. Wear test methodology

Six smooth discs, all with an R_a of less than 0.02 μm, were scratched using a diamond-tipped stylus. The diamond had a conical tip with a full cone angle of either 30, 60, 90 or 120 degrees. Table I shows the diamonds and loads used to make 12 equispaced radial scratches on each disc.

TABLE I Diamond cone angle and loads used to scratch the discs

Disc	Diamond cone angle (deg)	Load (N)
1	60	0.16
2	30	0.16
3	90	0.28
5	120	0.28
6	90	0.40
7	120	0.40

Each scratch was then characterized using a non-contacting UBM microfocus laser profilometer. The mean heights, widths and aspect ratios of the scratch lips were determined for each disc by measuring each three-dimensional scratch profile at seven cross-sections. The volume of scratch material above the zero reference plane was calculated and hence the average cross-sectional area of the scratch above the reference plane was determined. In addition, an unscratched disc was used in the wear tests to gain control data. The pins were marked prior to the test to record sliding direction, and the pin wear face was microtomed to remove residual strains caused by machining. Before and after each test, the pins and discs were cleaned in isopropanol in an ultrasonic bath for 5 min. After the tests, measurements of the discs' R_a were carried out on a Rank Taylor Hobson Talysurf 6. After being left to dry-out for two days in a temperature controled environment to stabilize the moisture content, the pins were weighed to an accuracy of $\pm 5\,\mu g$. After each test, the discs were inspected for evidence of transfer film.

A change in velocity has been shown to have no substantial effect on the wear of the surfaces when they are operating in the boundary or mixed lubrication regime [12]. Therefore the tests were carried out at a sliding velocity of $70\,mm\,s^{-1}$, which is substantially higher than physiological sliding rates. The sliding distance was approximately 13 km per test (note: 20 km is equivalent to one year of normal operation of the joint *in vivo*). The load was 80 N per pin, which corresponded to a 12 MPa nominal contact stress.

The tests were carried out in a solution of 100% bovine serum with sodium azide (0.02% w/v). At the end of each test, the serum was collected and frozen for isolation and characterization of the wear debris.

The wear factor, K ($mm^3\,Nm^{-1}$) [13], was calculated from the weight loss of the pins and converted to volume loss, applied load and sliding distance as follows

$$K = \frac{V}{PX} \tag{1}$$

where V is volume (mm^3), X is the sliding distance (m), and P is the normal load (N).

2.2. Wear debris isolation and characterization

The method recently developed at Leeds University [14] to isolate wear debris from the serum and characterize the particles is briefly described below. Serum (150 ml) was digested with 12 M potassium hydroxide for two days. Lipid was extracted with chloroform and methanol (2 : 1; 150 ml) over 24 h. The serum was centrifuged for 15 min (1300 g) and the supernatant was decanted into ice-cold ethanol and stirred at 4 °C to precipitate the proteins. This solution was then centrifuged for 2 h (2000 g). The supernatant was diluted to 0.75 M-KOH with non-pyrogenic water and sequentially filtered, through a 10 μm and a 0.1 μm pore preweighed polycarbonate filter. The filters were dried for at least 4 h under infrared lamps in a temperature controled environment and weighed. A random section of the filter was cut out, away from the edge and center of the filter and gold coated. The filter was viewed by scanning electron microscopy (SEM, Hitachi S-700) and images collected. The debris was then sized by image analysis (Image Pro Plus 3.0). The key parameters used to characterize the debris were particle number, aspect ratio, perimeter and area. Over 100 particles were characterized for each sample.

2.2.1. Statistical analysis

The results were analyzed by one-way ANOVA and the minimum significant difference between means was calculated by the T-method ($p < 0.05$) [15].

To test the relationship between two parameters the product–moment correlation coefficient was calculated [16].

2.3. Finite element analysis

A finite element method was used to analyze the effect of the scratch lip geometries on the surface strains in the UHMWPE.

A two-dimensional plane strain finite element analysis of the cyclic deformation of UHMWPE by a counterface asperity was conducted using ABAQUS version 5.4 [17]. The model consisted of an otherwise smooth and flat stainless steel surface containing a single asperity, representing the lip of a typical scratch found on a series of 12 explanted Charnley stainless steel femoral heads, in contact with a semi-infinite block of UHMWPE, representing the acetabular cup. Fig. 1 shows a contour plot of the lateral area of an explanted femoral head, with both deep and fine scratches. The defects on the surface were found to be long, in most cases over 300 μm, and also fairly straight. Therefore it was reasonable to model the defect in a two-dimensional plane strain finite element analysis, with the sliding velocity perpendicular to the long axis of the scratch, since this was the direction of sliding most likely to induce wear and damage in the polymer. The height and width of the asperities formed by the lips either side of the surface scratches were determined by measuring typical scratches on the explanted Charnley femoral heads. These measurements were taken using a Rank Taylor Hobson Talysurf 6 profilometer and gave a mean scratch lip height of 1.1 μm, while the mean half width was 15 μm. The geometry was made non-dimensional by defining an asperity aspect ratio as the asperity height divided by the half width (Fig. 2), resulting in a mean aspect ratio (height divided by half width) of 0.08 [11]. These three parameters were used in the finite element analysis to model typical asperities on the stainless steel contact surface. Thus the FEA modeled an asperity with a range of heights between 1 and 4.1 μm with a constant width of 50 μm, and a range of widths between 7 and 20 μm with a constant height of 1 μm. In addition, a range of heights and widths with a constant aspect ratio of 0.125 were modeled.

The scale of the asperity was of the order of micrometers. Therefore, compared to the radius of curvature of a femoral head and acetabular cup, which is of the order of millimeters, both surfaces could be modeled as flat. In addition, due to the differences in wavelength of the respective surface defects, it was

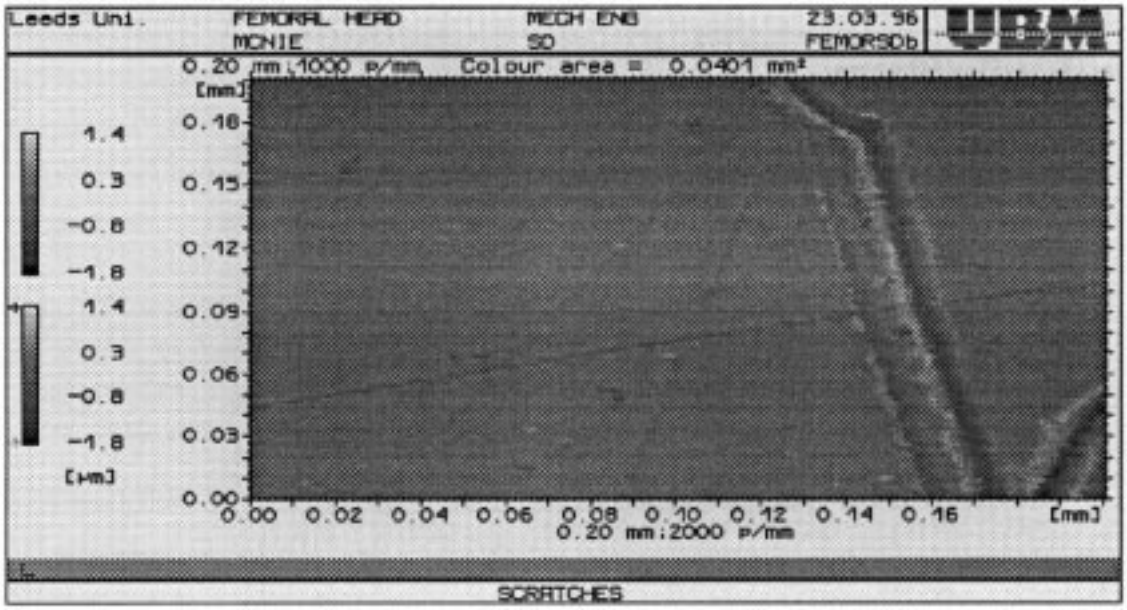

Figure 1 Contour plot of the lateral section of a femoral head.

assumed that the UHMWPE was smooth compared to the metal. Hence the interaction of UHMWPE with a microscopic metallic counterface asperity [9] was reduced to a relatively simple model.

The contact between the two surfaces was simulated by pressing the asperity into the UHMWPE by its full height and then allowing the two surfaces to slide over a distance of 150 µm, at a relative velocity of 22 mm s^{-1}. This is the average sliding speed of a Charnley stainless steel head *in vivo* [13]. The models have been described in more detail by McNie *et al*. [11]. Five types of model were studied:

1. A single pass of two stainless steel asperities separated by 10 µm, defined to have a constant width of 50 µm and a range of heights, or a constant height of 1 µm and a range of widths.
2. Multiple passes of a single asperity defined to have a constant height of 1 µm and a range of widths. The surfaces were allowed to slide and then the direction of sliding was reversed, until the surfaces were back to their initial position. This cyclic sliding of the asperity over the UHMWPE surface was repeated up to 11 times.
3. A single pass of a single asperity, defined to have a constant height of 1 µm and a range of widths.
4. A single pass of a single asperity, defined to have a constant width of 50 µm and a range of heights.
5. A single pass of a single asperity, defined to have a constant aspect ratio of 0.125 with a range of heights and widths.

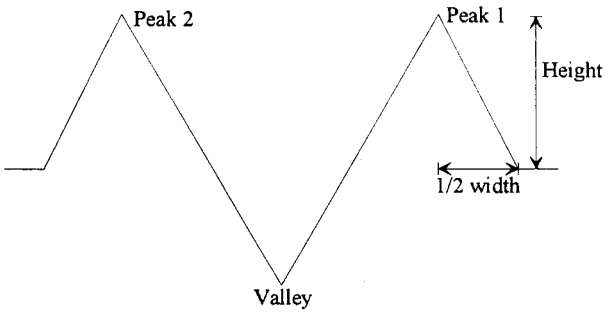

Figure 2 Geometry of typical scratches.

Three key parameters were studied for each model and investigated as indicators of wear:

1. The cross-sectional area of UHMWPE being strained plastically, A_1.
2. The plastic strain area integral, $\int \varepsilon dA_1$, which is an indicator of the risk of fatigue crack initiation.
3. The maximum plastic strain, ε_{max}, and its position.

3. Results

3.1. Surface characterization of wear test discs

The scratches produced on the discs to simulate third body damage were characterized using a three-dimensional non-contacting profilometer. A section of a typical scratch on a disc is shown in Fig. 3.

An idealized scratch profile is shown in Fig. 2 on which the reference points that were measured are highlighted. The scratches on the wear test discs had mean geometries as given in Table II. The two-dimensional area measurement (Table II) was the average cross-sectional area of the scratch lip above the mean zero line. Generally, the scratch lips were similar in height to the asperities modeled in the FEA; however, higher aspect ratios, up to 0.8, were measured.

There was little increase in the surface roughness, R_a, measured between the scratched regions, before and after the test. The R_as were always less than 0.02 µm, which is the upper tolerance for the manufacture of stainless steel femoral heads. Hence the discs were considered to remain smooth throughout the test (apart from the scratched regions).

3.2. Wear test results

The results were analyzed by one-way ANOVA and a minimum significant difference of 2.5×10^{-8} mm^3

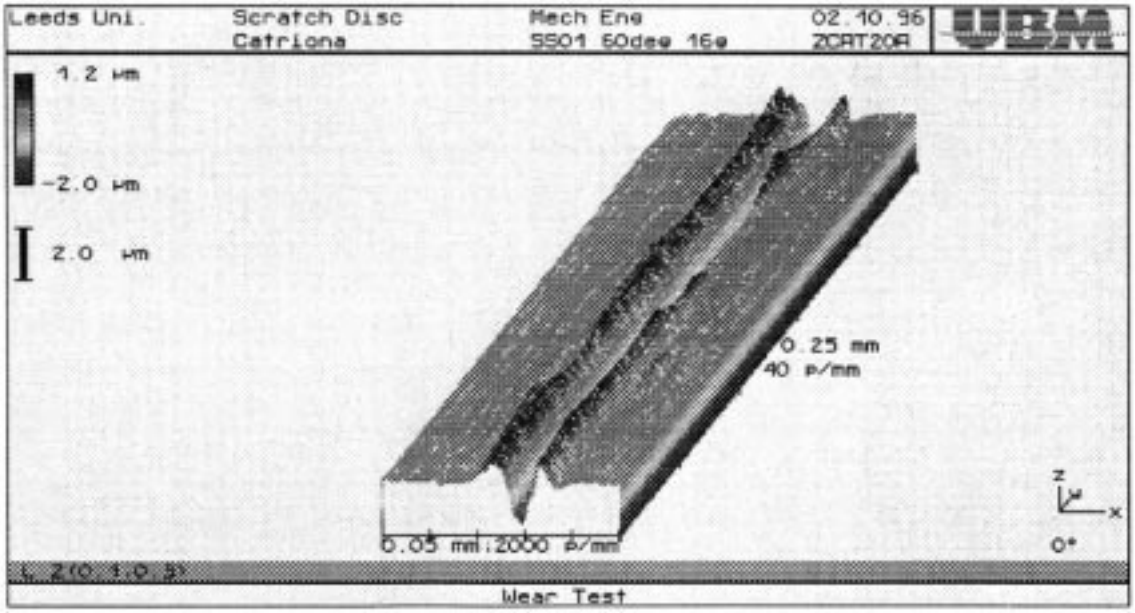

Figure 3 Typical profile of a section of a scratch on a stainless steel counterface made with a diamond.

TABLE II Summary of scratch profiles

Disc/diamond angle (deg)	Half width (μm)	Height (μm)	Aspect ratio	Two-dimensional area (μm^2)
1/60	2.432	1.222	0.513	5.87
2/30	1.509	0.861	0.575	2.60
3/90	2.501	1.971	0.802	9.86
5/120	1.998	1.365	0.634	5.91
6/90	3.8727	1.827	0.554	13.02
7/120	4.166	1.148	0.295	9.37

TABLE III Aperity cross-sectional areas and the wear factors

Disc	Two-dimensional area (μm^2)	Wear factor $\times 10^{-8}$($mm^3\,Nm^{-1}$)
2	2.60	1.03
4	0	1.75
5	5.91	2.58
1	5.87	3.32
7	9.37	3.33
3	9.86	4.3
6	13.02	11.4

Nm^{-1} was calculated. Table III shows the mean wear factors for the different discs. It can be seen from Table III that wear factors for discs 4 and 2 were significantly lower ($p < 0.05$) than those for discs 3 and 6. In addition, all the factors were significantly lower ($p < 0.05$) than the wear factor for disc 6. However, the other wear factors were not significantly different from each other.

The results of the wear tests are shown in Figs 4–6 plotted against the different mean geometric parameters measured on the surface of the scratched discs. It can be seen from Fig. 4 that an increase in the average cross-sectional area of the counterface scratch lip above the mean surface increased the wear factor (correlation coefficient, 0.81). Moreover, a somewhat weaker relationship between wear factor and scratch lip height was also found (correlation coefficient, 0.62), as shown in Fig. 5. A similar relationship was also found between wear factor and scratch lip width (correlation coefficient, 0.62). However, there was virtually no relationship

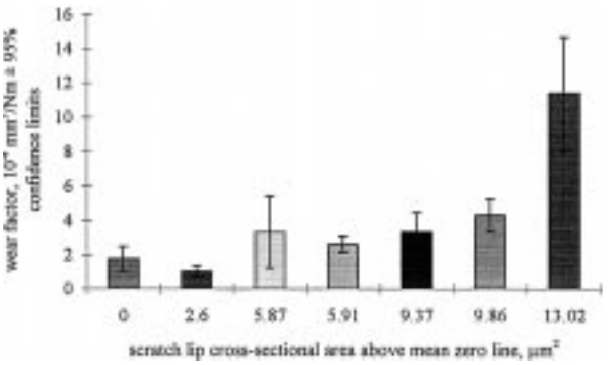

Figure 4 Variation of wear factor with scratch lip average cross-sectional area.

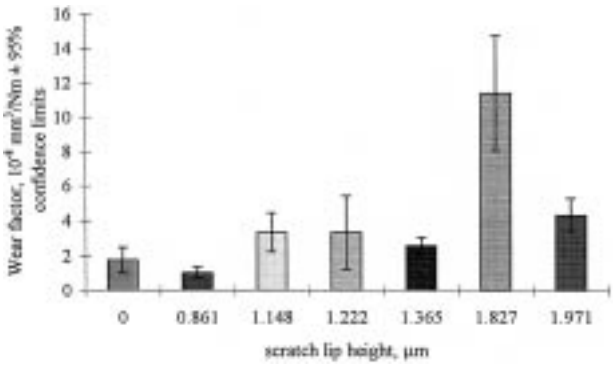

Figure 5 Variation of wear factor with scratch lip height.

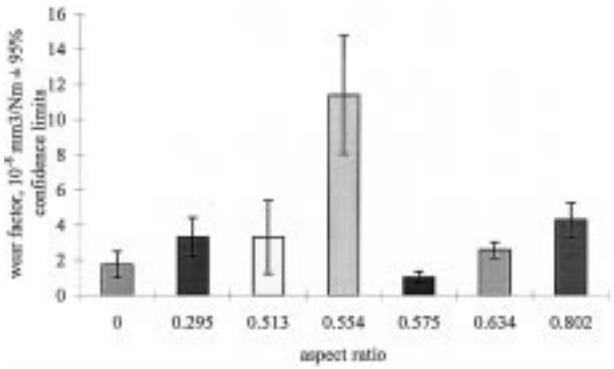

Figure 6 Variation of wear factor with scratch lip aspect ratio.

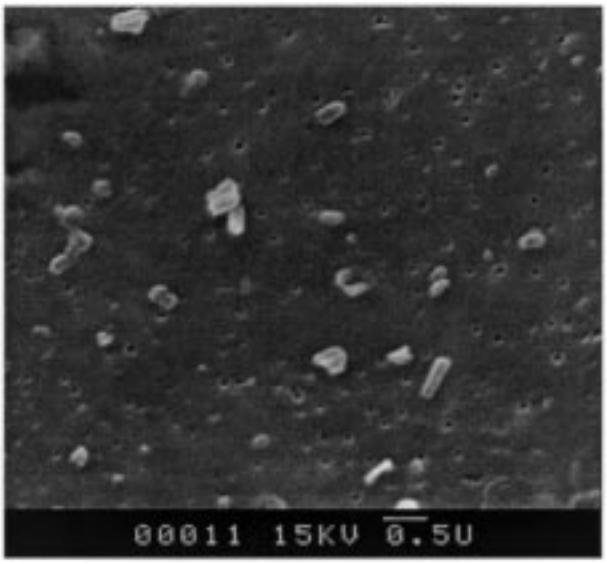

Figure 7 Typical debris, below 10 μm in mean size, from the wear test discs.

between wear factor and scratch lip aspect ratio, as shown in Fig. 6 (correlation coefficient, 0.25).

3.2.1. Wear debris analysis

An example of the filtered debris, less than 10 μm in mean dimension, is shown in Fig. 7. Analysis of the debris produced during the wear tests showed that the mode of the particle size distribution was in the range 0.1–0.5 μm for all the tests. An example of the size distribution of wear debris is shown in Fig. 8.

Fig. 9 shows that there was an increase in the percentage mass of debris below 10 μm as the aspect ratio of the scratch lip increased, with a correlation coefficient of 0.7. The lowest percentage mass of this small debris occurred with the smooth control disc (zero aspect ratio). There was a weaker correlation between an increase in scratch lip height and percentage mass of debris below 10 μm (correlation coefficient, 0.64).

Fig. 10a shows debris in the submicrometer range from a low scratch lip aspect ratio test (disc 7), while Fig. 10b shows corresponding debris from a high scratch lip aspect ratio test (disc 3). The debris morphology in this size range was different in the two cases, with generally smaller and rounder submicrometer-sized particles from the lower scratch lip aspect ratio tests.

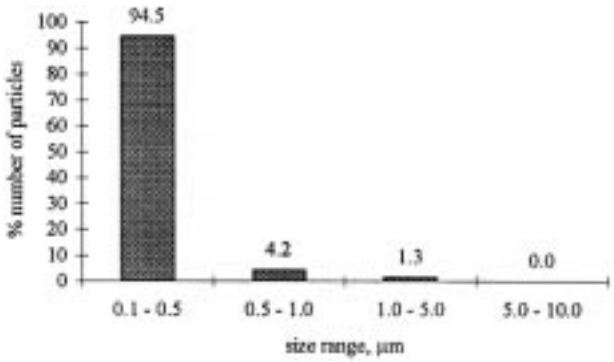

Figure 8 The typical debris size distribution of debris from the discs as a function of the area of the particle.

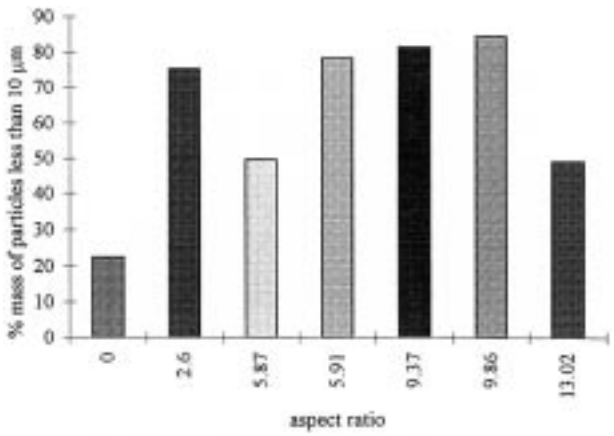

Figure 9 Variation of per cent mass of submicrometer particles with scratch lip aspect ratio.

3.2.2. Wear surface analysis

SEM analysis of the pin surfaces showed that there was generally more damage, in the form of ripples perpendicular to the sliding direction on the surfaces of pins, for sliding against higher aspect ratio scratch lips. Fig. 11a shows a pin surface from a low aspect ratio (0.295) wear test (disc 7) with little orientation and Fig. 10b shows the ripple effect on the pin surface from a high aspect ratio (0.802) wear test (disc 3).

3.3. Finite element analysis

It had previously been found [11] that there was a strong non-linear relationship between the magnitude of the maximum plastic strain predicted by the FEA in the UHMWPE and the height or width of a single counterface asperity. It is now shown in Fig. 12(a, b) that when two asperities were modeled, representing a typical complete single scratch geometry, there was little difference in the maximum predicted plastic strains compared with these strains predicted when only a single asperity of the same geometry was modeled. The area of plastic strain after a single pass of the asperity was not significantly different for the single or double asperity model. Therefore, for simplicity, a single asperity was considered in all future models.

Contour plots of the plastic strain accumulation predicted by the finite element model after eight cycles of sliding of a single asperity, 1 μm in height for asperity widths of 18 and 10 μm, over the UHMWPE surface are

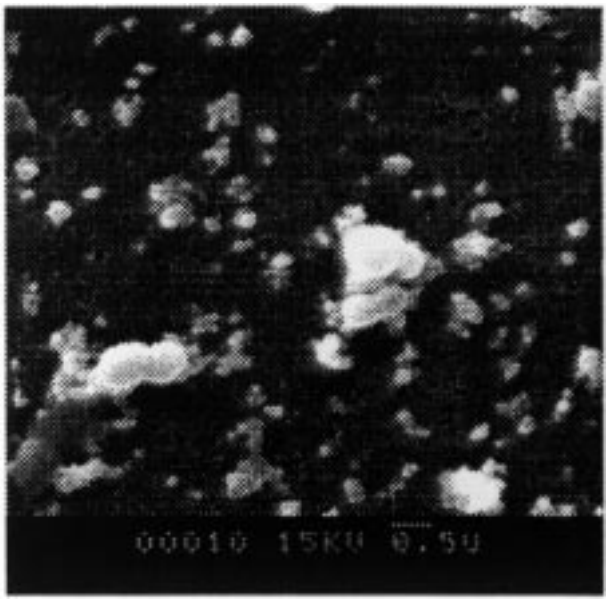

(a)

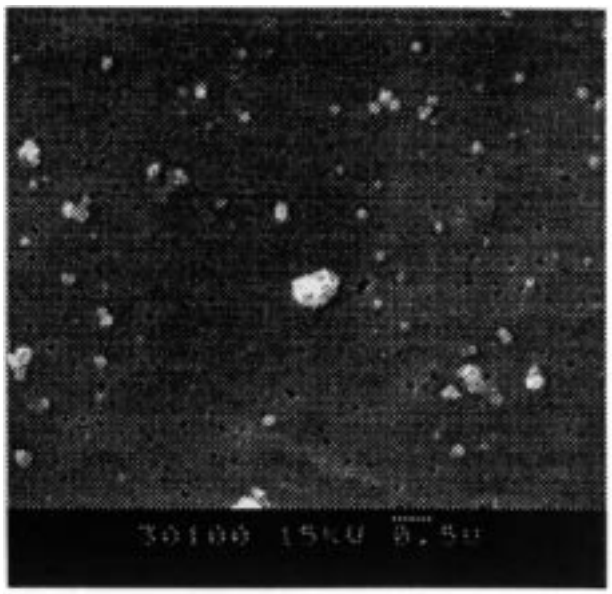

(b)

Figure 10 SEM micrographs showing debris from (a) low and (b) high scratch lip aspect ratio tests, respectively.

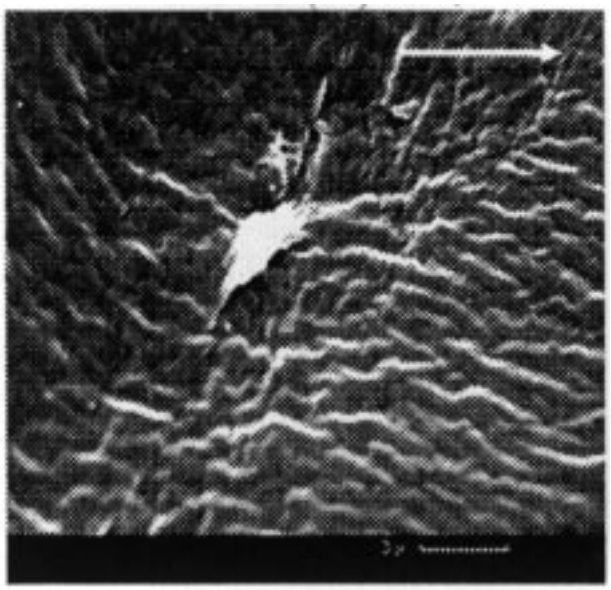

(a)

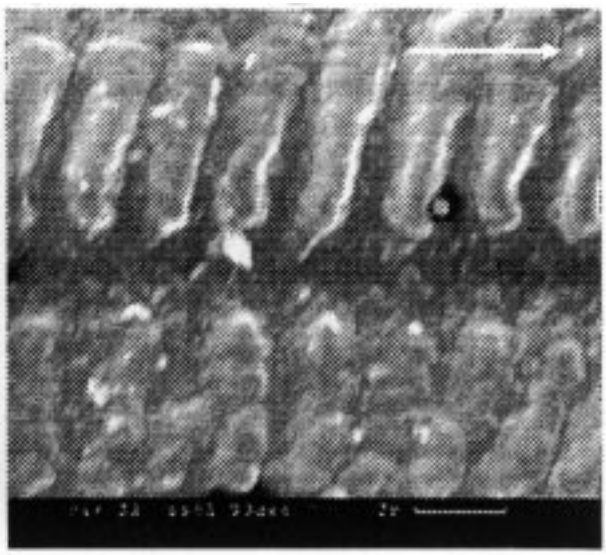

(b)

Figure 11 SEM micrographs of pin surfaces from (a) low and (b) high scratch lip aspect ratio tests, respectively.

shown in Fig. 13(a, b), respectively. It can be observed that the maximum plastic strain reduced with increased asperity width but remained close to the surface of the UHMWPE for both cases. Conversely, the size of the region of UHMWPE undergoing plastic strain increased with increased asperity width.

The maximum plastic strains during successive passes of a single asperity, with a constant height of 1 μm and varying width in the range 7–20 μm, are shown in Fig. 14. The FEA predicted that the magnitude of the plastic strain in the polymer increases non-linearly with decreasing width and consequently with decreasing cross-sectional area of the asperity, during the first cycle. In subsequent cycles the incremental increases in the maximum plastic strain reduced but the same overall trend remained. The area of plastic strain decreased with decreasing width and area of the asperity. However, this area remained constant throughout the cycles. Since it was apparent that the relative effect of aspect ratio remained the same after eight cycles as for a single pass analysis, only the single pass results have been used for further comparisons.

Fig. 15(a, b) shows that the area of UHMWPE undergoing plastic strain due to the asperity contact increased with both increasing width and height of the asperity. These dimensions could be combined into one geometrical parameter, asperity cross-sectional area. Thus the area of plastic strain increased approximately linearly with increasing asperity cross-sectional area, Fig. 15c, with the best-fit relationship

$$A_1 = 24.3A_2 + 321.3 \qquad (2)$$

where A_1 is the area of plastic strain and A_2 is the asperity area. It is demonstrated in Fig. 15d that there was no simple relationship between plastic strain area and asperity aspect ratio.

Fig. 16(a–d) shows the integral of plastic strain with respect to the area of UHMWPE undergoing this plastic strain plotted against asperity width, height,

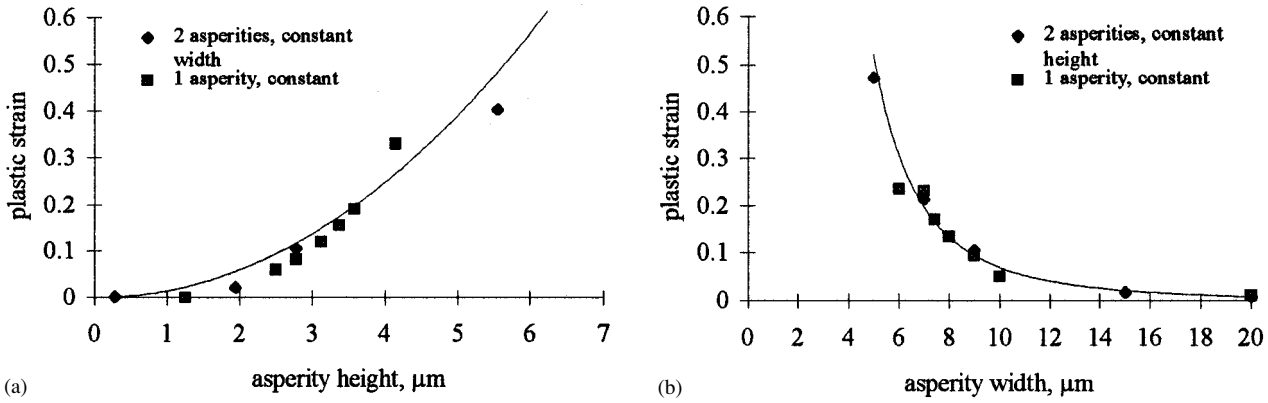

Figure 12 Maximum plastic strains for asperities of different geometries and of different height (a) and width (b).

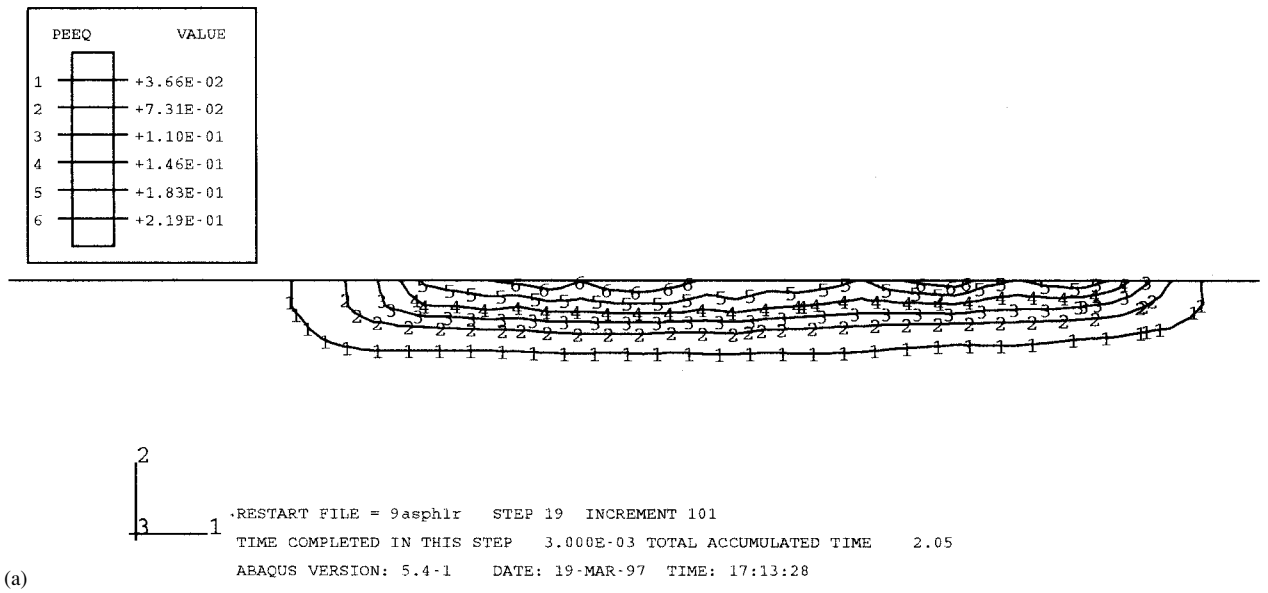

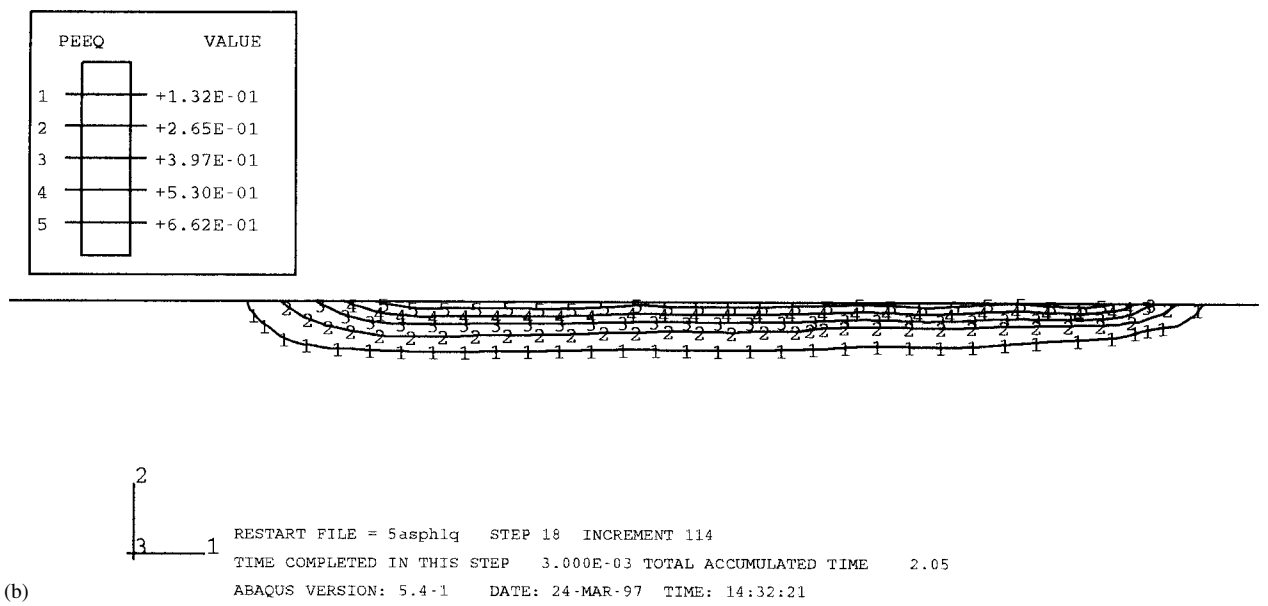

Figure 13 Contour plot of plastic equivalent strain for models with aspect ratios of 0.11 (a) and 0.2 (b) after eight cycles.

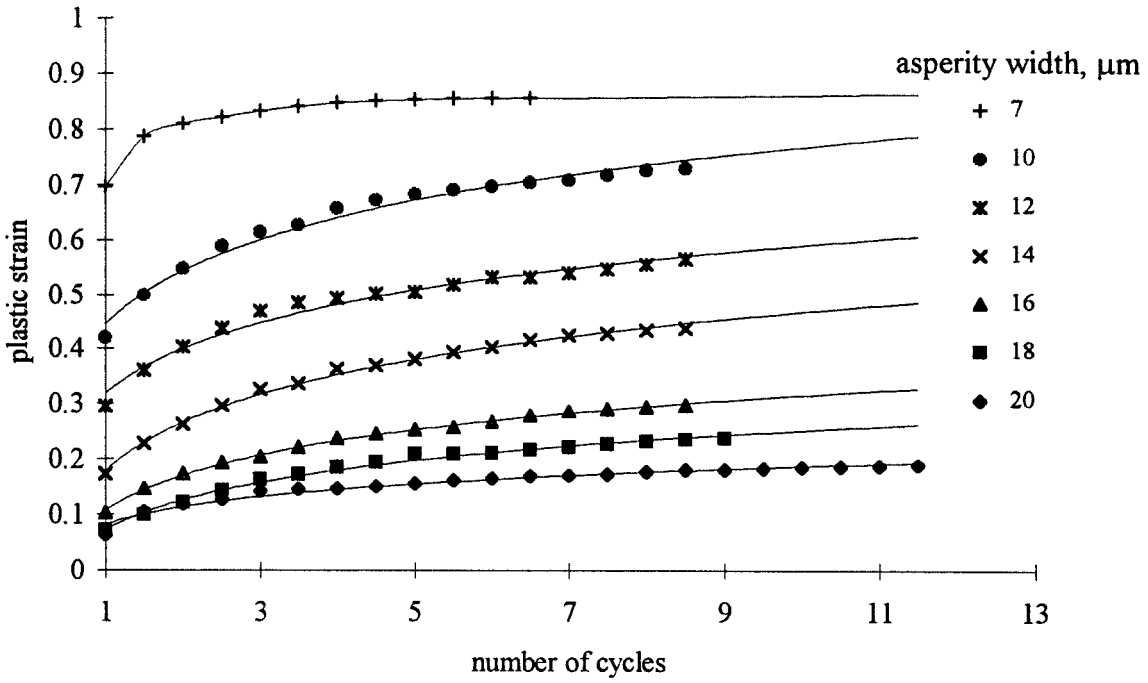

Figure 14 Cyclic plastic strain accumulation for different asperity aspect ratios (in micrometers).

cross-sectional area and aspect ratio, respectively. This integral can be used to give an indication of the risk of fatigue crack initiation. It can be seen that the effect of increasing width asperity was to reduce this integral slightly, while increasing the asperity height increased the integral. When the height and width were combined to give the asperity cross-sectional area, the plastic strain area integral generally increased with increasing asperity area as the increase in asperity height had a more dominant effect with the best-fit relationship

$$\int \varepsilon dA_1 = 3.09hw + 38.96 \qquad (3)$$

In this expression is defined as the plastic strain, h is defined as the asperity height and w as the asperity half width. However, there is no unique relationship between

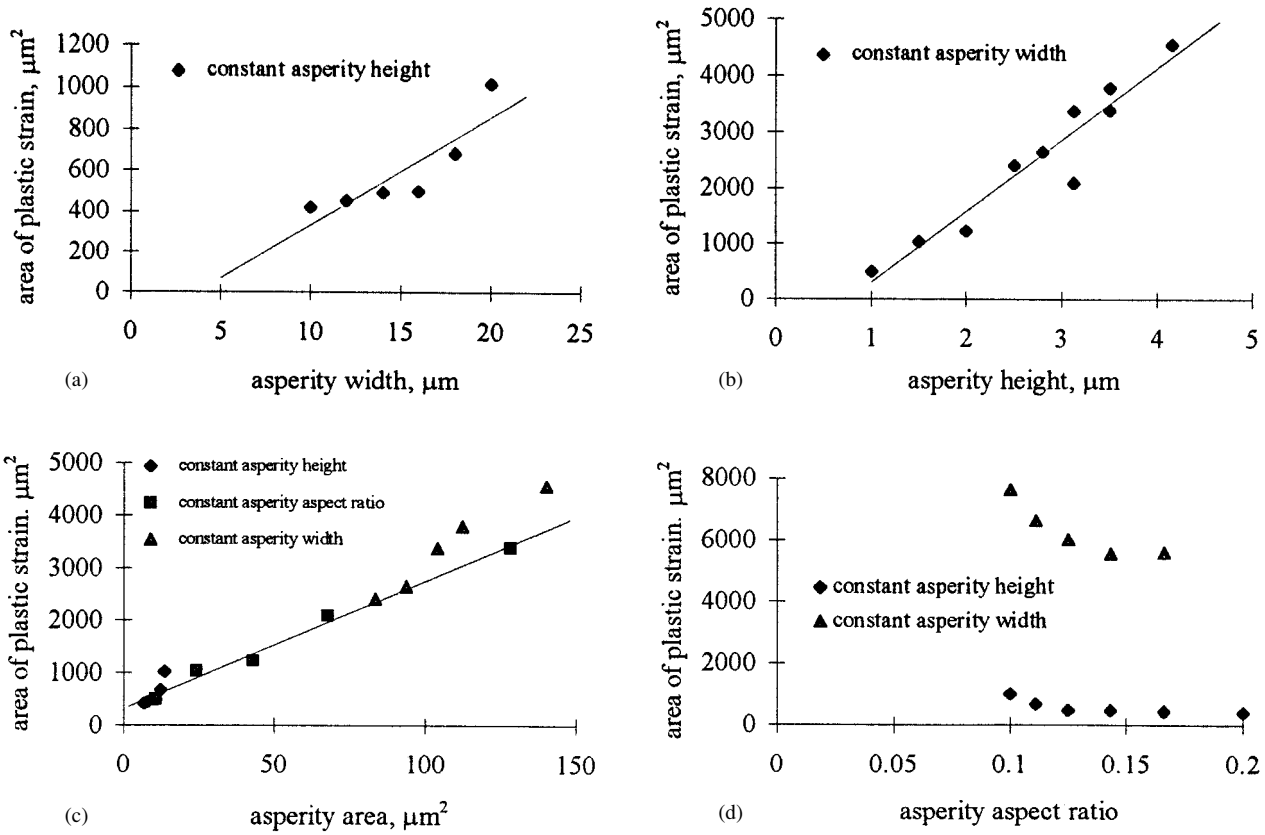

Figure 15 The variation of the area of plastic strain with (a) asperity width, and (b) asperity height, (c) asperity area, and (d) asperity aspect ratio.

the plastic strain area integral and aspect ratio due to the dominance of asperity height, Fig. 16d.

Fig. 12(a, b) shows how the value of maximum plastic strain varied with either increasing width or height of the asperity. This could be combined into one geometrical parameter, aspect ratio, which is the height divided by the half width of the asperity and it can be seen from Fig. 17a that the plastic strain increased non-linearly with increasing aspect ratio regardless of asperity size, as found previously in [11] for a smaller range of aspect ratios. The best-fit relationship was

$$\varepsilon_{max} = 35.6\left(\frac{h}{w}\right)^{2.7} \quad (4)$$

It was also found that when the aspect ratio was held constant the maximum plastic strain very nearly remained constant regardless of the actual dimensions of the asperity. A simple relationship was not found between maximum plastic strain and asperity area, Fig. 17b.

Fig. 18 shows the plastic strain distribution as a function of depth for single asperities of varying aspect ratio but constant height. It can be seen that the position of maximum strain moves closer to the surface as the

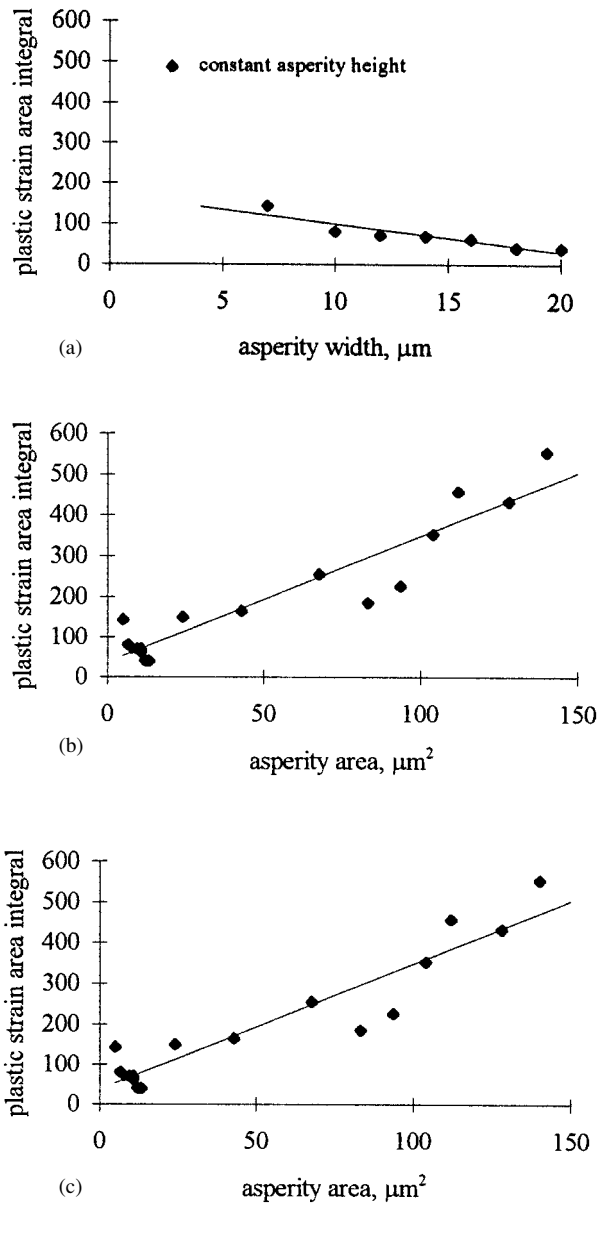

Figure 16 The variation of the plastic strain area integral with (a) asperity width, (b) asperity height, (c) asperity area, and (d) asperity aspect ratio.

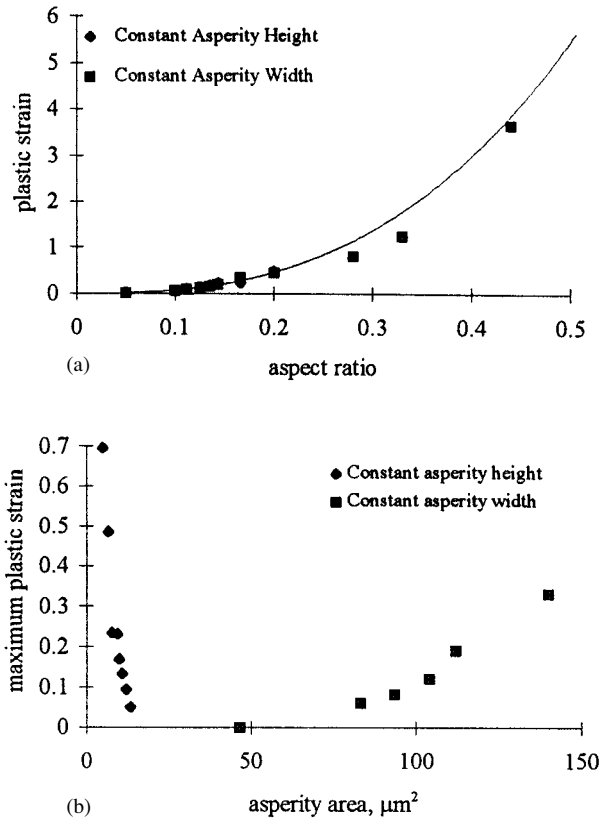

Figure 17 Variation of maximum plastic strain with (a) asperity aspect ratio, and (b) asperity area.

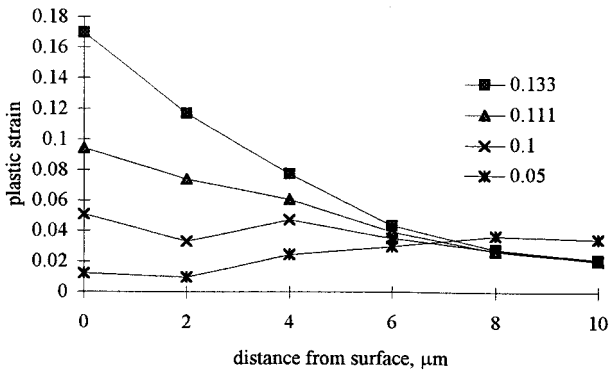

Figure 18 Variation of the plastic strain through the UHMWPE at different aspect ratios.

aspect ratio of the asperity increases. Moreover, the value of maximum strain increased significantly as the aspect ratio increased.

4. Discussion

Clinically there is evidence that hard small particles have the potential to cause scratches of typical lip height, 1 μm [18–20]. Surface characterization of a series of explanted Charnley femoral heads found a mean scratch lip height of 1 μm, while the mean aspect ratio (height–half width) of these scratch lips was found to be 0.1. It has been shown in previous laboratory wear tests that it only requires a single scratch of this scale to produce a large increase in wear factor [21]. Fig. 1 shows wide variation in scratch types, both deep and fine, and it is probable that the different scratches were created by different processes, which have not at present been firmly identified. However, it may be that an abrasive action occurs in two different modes, wedging and ploughing. The wedge mode would give the larger scratches and the ploughing mode would result in the finer scratches due to an increased sharpness of the defect. Bone, cement and/or metallic particles may have caused the scratches, though it is as yet unclear which particles caused each type of scratch.

The wear tests have shown that the average cross-sectional area of the counterface scratch lip was the dominant geometrical factor in governing the overall wear volume. In support, the FEA results showed that, when the area of the asperity above the mean line increased, the size of the plastically deformed region increased linearly (Equation 2). Thus the probability of defects in the UHMWPE initiating low cycle fatigue was increased leading to increased wear volumes. This trend was also reflected by the plastic strain area integral (Equation 3). These results indicated that the wear volume may be more closely related to the area undergoing plastic strain and the plastic strain area integral, rather than to the maximum value of plastic strain.

The FEA results showed that the area undergoing plastic strain and the plastic strain area integral were independent of the asperity aspect ratio. Similarly, the wear tests showed that wear volume was not dependent on scratch lip aspect ratio. Thus both results indicate that the asperity aspect ratio is not a critical determinant of the amount of wear. Abrasive microscopic wear has been found to be proportional to the slope of the asperity on a counterface surface [22], but the increase in asperity slope may also increase the asperity cross-sectional area, as asperity widths tend to remain fairly constant. Hence the abrasive wear rate may also be related to the asperity volume, supporting both the finite element results and the wear test results.

The FEA results predicted that the maximum value of plastic strain did depend on aspect ratio (Equation 4). This relationship between maximum plastic strain and aspect ratio was reflected in the surface damage and ripples found on the SEM micrographs of the surfaces of some of the wear pins; these ripples becoming more dominant with increasing aspect ratio. It is probable that, as the scratch lip aspect ratio increased, higher strains occurred on the surfaces, as predicted by the FEA, creating the ripple effects. This surface damage was observed by Wang *et al*. [23] and is believed to be a result of surface fatigue wear. Dowling *et al*. [24] also observed the same ripples on the surfaces of explanted UHMWPE acetabular cups, particularly in areas of high wear. It is interesting to note that, in hip joint simulators using non-irradiated UHMWPE, high surface and subsurface plastic strains were apparent, but ripples were not observed [25].

In the present wear tests, no difference in the particle size frequency distribution was found for different scratch geometries. This is not surprising as the test is not a sensitive method for differentiating particles. However, a definite trend (correlation coefficient of 0.7) of increasing percentage mass of debris less than 10 μm in size with increasing scratch lip aspect ratio was found. This may have been due to the high aspect ratio scratch lips causing higher magnitude surface strains, as predicted by the FEA and observed on the pin surfaces, leading to a high rate of surface wear, and hence more submicrometer-sized particles. This was also supported by the FEA results in Fig. 18, which showed that, at higher asperity aspect ratios, the higher surface strains were combined with high strain gradients. In contrast, for lower aspect ratio scratch lips, subsurface strain accumulation was more likely to occur since the FEA predicted relatively higher subsurface strains, as shown in Fig. 18. Hence a ratcheting subsurface strain accumulation mechanism was predicted to be the dominant wear mechanism, which is likely to produce larger particles. Therefore the FEA results were indicative of a greater percentage mass of large debris for low aspect ratio scratch lips, as found experimentally.

With larger aspect ratio asperities, a more severe surface action is likely to occur as the finite element model predicted much higher surface strains. Hence a low cycle surface fatigue or abrasive mechanism was predicted to be the dominant wear mechanism for high aspect ratio scratch lips, which can produce smaller particles.

Rougher scratched surfaces generally have higher aspect ratio scratch lips than smooth surfaces [22] due to the scratch height increasing and width remaining fairly constant. Consequently, these trends of particle morphology support the qualitative observations made by Hailey *et al*. [8] that smoother surfaces were more likely to generate larger platelet-type particles. Other finite element analyses have modeled the interaction of two triangular asperities and considered the mode of failure [26]. The results predicted that the size of the particle is inversely proportional to the aspect ratio of the steeper of the two asperities if the slope of the other is very large, which supports the findings from the present finite element study.

As shown by the present wear tests, a larger percentage mass of particles greater than 10 μm was generated by low aspect ratio scratch lips. However, with small particles still being produced at the surface in the low aspect ratio test, a bimodal mass distribution resulted. Interestingly, the smallest submicrometer-sized particles from low aspect ratio tests, Fig. 10a, were found to be generally smaller and rounder than debris from the

higher aspect ratio wear tests. This implies that, as the asperity aspect ratio increases, the particles generated increase in number, become more irregular and slightly larger but, most importantly, remain primarily submicrometer.

5. Conclusions

This study aimed to investigate theoretically and experimentally the influence of scratch lip geometry on wear rate and debris morphology in UHMWPE artificial joints.

In the wear tests, an increase in scratch size as indicated by a greater cross-sectional area of the scratch lip above the mean line caused an increase in wear volume. This was supported by a predicted increase in the area of plastic strain and plastic strain area integral with asperity cross-sectional area from the FEA.

On the other hand, the high rate of surface plastic strain accumulation predicted by the FEA for high aspect ratio asperities in this study offers an explanation for the increased quantities of submicrometer-sized wear particles compared to lower aspect ratio wear tests. This is particularly important as many small sharp scratches are found frequently on the surface of explanted femoral heads, and these could well be responsible for an increased incidence of submicrometer-sized wear particles leading to osteolysis.

The above results indicate that a full characterization of the wear counterface is required, taking into account both the shape and size of scratch lips, as these scratch lip parameters can be considered useful predictors of osteolytic potential.

Acknowledgments

This work has been supported by the Wellcome Trust, and the DTI CAM 1 Project.

References

1. H. AMSTUTZ, P. CAMPBELL, N. KOSSOVSKY and I. CLARKE, *Clin. Ortho. Rel. Res.* **276** (1992) 7.
2. J. CHIBA, W. MALONEY, M. HORIKOSHI, L. MCINTYRE and H. RUBASH, in ''Proceedings of the 39th Annual Meeting of the Orthopaedic Research Society'', Vol. **22-2** (1997) p. 270.
3. T. GREEN, J. FISHER and E. INGHAM, in ''Transactions of the 42nd Annual Meeting of the Orthopaedic Research Society'', (Orthopaedic Research Society, 1997) p. 733.
4. A. SHANBHAG, J. JACOBS, T. GLANT, J. L. GILBERT, J. BLACK and J. O. GALANTE, *J. Bone Joint Surg.* **76-B** (1994) 60.
5. P. CAMPBELL, S. MA, B. YEOM, H. A. MCKELLOP, T. P. SCHMALZREID and H. C. AMSTUTZ, *J. Biomed. Mater. Res.* **29** (1995) 127.
6. J. L. HAILEY, E. INGHAM, J. FISHER, D. DOWSON and B. M. WROBLEWSKI, in ''Proceedings of the 11th European Conference on Biomaterials'', (1994) pp. 321–3.
7. K. KATO, in ''New Directions in Tribology'', edited by I. M. Hutchings (MEP, London, 1997).
8. J. L. HAILEY, E. INGHAM, M. STONE, B. M. WROBLEWSKI and J. FISHER, *Proc. Inst. Mech. Eng. Part H* **210** (1996) 3.
9. J. FISHER, *Current Orthopaedics* **8** (1994) 164.
10. J. A. ESTUPINAN, D. L. BARTEL and T. M. WRIGHT, in ''Transactions of the 42nd Annual Meeting of the Orthopaedic Research Society'', (Orthopaedic Research Society, 1996) pp. 48–8.
11. C. M. MCNIE, D. C. BARTON, M. H. STONE and J. FISHER, *J. Eng. Med.* **212** (1998) 49.
12. J. FISHER, D. DOWSON, H. HAMDZAH and H. LEE, *Wear* **175** (1994) 219.
13. J. H. DUMBLETON in ''Tribology of Natural and Artificial Joints'', (Elsevier, New York, 1981) p. 50.
14. J. L. TIPPER, E. INGHAM, J. L. HAILEY, A. A. BESONG, M. STONE, B. M. WROBLEWSKI and J. FISHER, in ''Transactions of the 43rd Annual Meeting of the Orthopaedic Research Society'', Vol. **22-1** (Orthopaedic Research Society, 1997) p. 355.
15. R. R. SOKAL and F. J. ROHLF, in ''Biometry'', (W. H. Freeman, New York, 1995) p. 244.
16. *Idem*., *ibid.* p. 560.
17. HIBBET, KARLSSON, SORENSEN, INC., ABAQUS Standard/User's Manual, Version 5.4 (1994).
18. L. CARAVIA, D. DOWSON, J. FISHER and B. JOBBINS, *Proc. Inst. mech. Eng. Part H* **204** (1990) 65.
19. M. JASTY, C. R. BRAGDON, K. LEE, A. HANSON and W. H. HARRIS, *J. Bone Joint Surg.* **76-B** (1994) 73.
20. J. R. COOPER, D. DOWSON and J. FISHER, *Wear* **162–164** (1993) 378.
21. J. FISHER, P. FIRKINS, E. A. REEVES, J. L. HAILEY and G. H. ISSAC, *Proc. Inst. Mech. Eng. Part H* **209** (1995) 263.
22. J. K. LANCASTER, in ''Friction and Wear'', edited by A. D. Jenkins (North Holland, 1972) pp. 960–1046.
23. A. WANG, V. K. ESSNER, D. C. SUN, C. STARK and J. H. DUMBLETON, in ''New Directions in Tribology'', edited by I. M. Hutchings (MEP, London, 1997) pp. 443–58.
24. J. DOWLING, J. R. ATKINSON, D. DOWSON and J. CHARNLEY, *J. Bone Joint Surg.* **60-B** (1978) 375.
25. J. R. COOPER, D. DOWSON and J. FISHER, *Wear* **151** (1991) 391.
26. L. M. KEER, Y. XU, H. S. CHANG and J. L. XUAN, *Tribology Trans.* **36** (1993) 613.

Received 26 February
and accepted 3 August 1998